Supporting Information

Enhancing visible-light photocatalytic performance of Au/TiO_2 catalysts through light reflection-promoted optical absorption with oriented anatase mesocrystals

Jingling Yang[1,2] Shiman He[2], Hongwei Liu[3], Esa Jaatinen[4], Eric Waclawik[4], Jiamin Quan[5], Sarina Sarina[4], Chun He[6], Senchuan Huang[2], Huaiyong Zhu[4,], Mingmei Wu[2,*]*

1 School of Environment, Jinan University, Guangzhou 510632, P. R. China.

2 School of Chemical Engineering and Technology/School of Chemistry, Sun Yat-Sen University, Zhuhai 519082/Guangzhou 510275, P. R. China.

3 Australian Centre for Microscopy & Microanalysis, the University of Sydney, Sydney NSW 2006 Australia.

4 School of Chemistry, Physics and Mechanical Engineering, Queensland University of Technology, Brisbane, QLD4001, Australia.

5 The Key Laboratory of Optoelectronic Technology & System, Education Ministry of China, Chongqing University 400044, China.

6 School of Environmental Science and Engineering, Sun Yat-Sen University, Guangzhou, 510275, P. R. China.

E-mail: ceswmm@mail.sysu.edu.cn

E-mail: hy.zhu@qut.edu.au

The **Supporting Information** includes:

3 Text

3 Tables

13 Figures

18 Pages

Text S1. Details of theoretical calculations.

Text S2. Details of the fabrication process of Au/meso-TiO_2.

Text S3. Details for the electron spin resonance (ESR) experiment.

Table S1. Data of inductively coupled plasma mass spectrometry (ICP-MS) measurements of samples.

Table S2. Composition of sulfur compounds in the reaction products after photocatalytic reactions.

Table S3. CH_3SH catalytic activity of Au/meso-TiO_2 compares with that of previously reported catalysts.[1-5]

Fig. S1. Schematic illustration of the synthesis method of meso-TiO_2 and p-TiO_2.

Fig. S2. XRD patterns of meso-TiO_2, p-TiO_2, Au/meso-TiO_2 and Au/p-TiO_2.

Fig. S3. (a) Top-view SEM image and (b) side-view image of meso-TiO_2, and (c) HRTEM image of Au/p-TiO_2. (d) Top-view SEM image and size distributions of Au, and (e) side-view image of Au/P25. (f) HRTEM image of Au/P25. (g, h) High-resolution TEM image of Au/meso-TiO_2.

Fig. S4. XPS spectra of Au/meso-TiO_2 and meso-TiO_2 samples.

Fig. S5. Nitrogen adsorption/desorption isotherms of Au/meso-TiO_2, Au/p-TiO_2 and Au/P25.

Fig. S6. The standard curve of Au concentration measured by ICP-MS.

Fig. S7. The model of Au NPs arrangement uses for light transmission calculation.

Fig. S8. (a) UV-vis absorption spectra of Ti foil. Mott−Schottky plots for (b) meso-TiO_2 and (c) p-TiO_2 at a frequency of 1 k Hz obtained in darkness.

Fig. S9. Photographs of the photocatalysis equipment used for (a) water splitting and for (b) gaseous CH_3SH oxidation, respectively.

Fig. S10. The CH_3SH adsorption performance of the as-synthesized samples under darkness.

Fig. S11. Cycling performance of (a) odorous CH_3SH removal and (b) H_2 evolution over Au/meso-TiO_2.

Fig. S12. (a) Photocurrent responses of Au/P25 at an applied potential of 0.8 V *vs.* Ag/AgCl in 0.5 M Na_2SO_4 aqueous solutions under visible-light irradiation ($\lambda > 430$ nm). (b) Reaction suppression by the chemical scavengers of reactive species $\bullet O_2^-$, •OH, e^- and h^+.

Fig. S13. Normalized electric field intensity distributions in the xz plane at 540 nm for Au NPs on <001> oriented anatase TiO_2.

Supplementary Texts

Text S1. Details of theoretical calculations

Calculations of visible light transmission through Au NPs on TiO_2

The collection of nanoparticles attached to the surface of the anatase-type was modelled as a single layer of 10 nm diameter Au NPs closely packed on the surface of the crystal (Fig. S1). The average light absorption cross-section for a 10 nm diameter Au NP immersed in water/ethanol solution is $\sigma = 1.88 \times 10^{-17}$ m^{-2}. The concentration of the NPs in the closely packed state is $N = 1 \times 10^{24}$ m^{-3}, and the layer thickness is $t = 10$ nm. The absorption coefficient of the layer is given by

$$\alpha = \sigma \times N = 1.88 \times 10^{7} m^{-1}.$$

The relative transmission of a light beam through the layer into the substrate is given by the Beer-Lambert law：

$$T = Exp[-\alpha t] = 0.82$$

Text S2. Details of the fabrication process of Au/meso-TiO_2.

Firstly, a plate of titanium foil (10 mm × 10 mm × 0.15 mm) was degreased by sonication in a mixture of acetone, 2-propanol and distilled water (1 : 1 : 1, v/v, 30 mL) for 0.5 h, and subsequently dried under a nitrogen stream. The acid vapor oxidation (AVO) reaction was carried out by placing the pre-treated Ti plate on a flat column positioned in the center of a Teflon cup (volume: 10 mL) containing 2.0 mL aqueous solution of hydrofluoric acid (1.0%,w_{HF}/w_{water}) shown in Fig. S1. The Ti plate served as both the titanium source and the substrate. The reaction was carried out at 140 °C for 12 or 60 h. After the autoclave cooled down naturally to room temperature, the plate was taken out of the cup, washed with deionized water, and dried naturally at ambient temperature. AVO reaction of 12 h is the best condition to form oriented anatase TiO_2 mesocrystal with nearly 100% <001> orientation, as reported in our previous work.[1]

Text S3. Details for the electron spin resonance (ESR) experiment.

The hydroxyl radicals (•OH) and superoxide radicals ($•O_2^-$) were detected using a Bruker A300-10-12 electron spin resonance spectrometer (ESR, Bruker, Germany) with a 150 W short arc xenon lamp as the irradiation light source and 5, 5-dimethyl-1-pyrroline N-oxide (DMPO) as a spin trap agent. For •OH detection, 5 mg of catalyst and 0.2 mmol DMPO were added to 2 mL deionized water and shaken to suspend the catalyst. For $•O_2^-$ detection, 5 mg of catalyst and 0.2 mmol DMPO were added in 2 mL methanol and oscillated to suspend the catalyst evenly, respectively. After 1 min photocatalytic reaction, the mixture was added to an ESR quartz tube for an ESR test. The measurement was conducted at room temperature under open-air conditions.

Table S1. Data of inductively coupled plasma mass spectrometry (ICP-MS) measurements of Au/meso-TiO_2, Au/p-TiO_2 and Au/P25.

Sample	Count per second (CPS)	Au loading amount (wt%)
Au/meso-TiO_2	5157.13056	2.0
Au/p-TiO_2	5160.13056	2.0
Au/P25	5414.73161	2.1

Table S2. Composition of sulfur compounds in the reaction products after photocatalytic reactions.

Catalyst	Removal efficiency of CH_3SH	Composition of the reaction products[a]		
		Surface adsorbed CH_3SH	$CH_3SO_3^-$	SO_4^{2-}
Au/meso-TiO_2	92.2%	4.6%	2.1%	85.5%
Au/p-TiO_2	51.0%	4.5%	7.3%	39.2%
Au/P25	69.9%	6.2%	4.3%	59.4%

Reaction condition: $[CH_3SH]_0$= 50 ppm, gas flow = 100 mL/min, 25 °C, reaction time = 20 min).

[a]Composition of the reaction products is calculated based on the molar ratio of products relative to the total introduced CH_3SH, respectively.

Table S3. CH_3SH catalytic activity of Au/meso-TiO_2 compares with that of previously reported catalysts.[1-5]

Catalyst	Conv.[a]	Ratio of CH_3SH /catalyst (mg/g)	Products	Amount of catalyst (g)	CH_3SH concentration and gas flux	Reaction time and temperature	Ref
Au/meso-TiO_2	92.2%	24.6	$CH_3SO_3^-$, SO_4^{2-}	0.008	50 ppm 0.1L/min	20 min, 25 °C	This work
Ag/MnO_2	95.0%	1.4	SO_4^{2-}, $HCOO^-$, CO_3^{2-}, CO_2	0.10	70 ppm 0.1L/min	10 min, RT[b]	8
g-C_3N_4/I^{3-}-BiOI	94.2%	12.4	$CH_3SO_3^-$, SO_4^{2-} ,	0.05	70 ppm 0.15 L min	30 min, RT[b]	9
Fe/Sludge-Derived Carbon	98.8%	0.2	SO_4^{2-}, $CH_3SO_3^-$	0.50	50 ppm 100 mL/min	10 min, RT[b]	10
Ag/g-C_3N_4	93.0%	8.9	CH_3SSCH_3	0.10	5 ppm 0.50 L/min.	3 h, RT[b]	11
Cr/Al_2O_3	98.0%	0.9	Not mentioned	0.20	100 ppm 30 mL/min	30 h, 375~425 °C	12

[a] The conversion rate (conv.) of CH_3SH.

[b] Room temperature (RT)

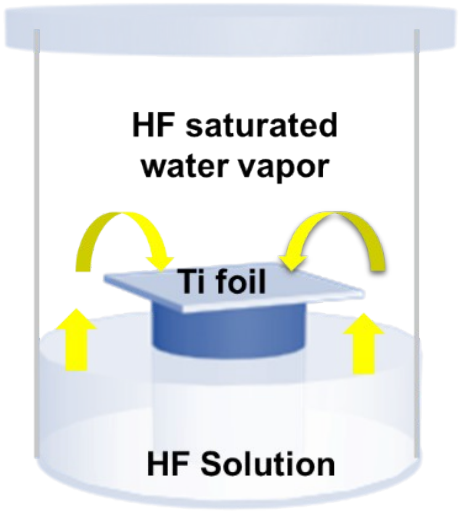

Fig. S1. Schematic illustration of the synthesis method of meso-TiO_2 and p-TiO_2.

After HF vapor oxidation for 12 h, the anatase TiO_2 mesocrystal vertically grown along the <001> direction (meso-TiO_2) was obtained. When the reaction time was further prolonged to 60 h, the smooth surface of oriented anatase TiO_2 was significantly dissolved, and a rough surface of polycrystalline TiO_2 nanoparticles (p-TiO_2) appeared.[1]

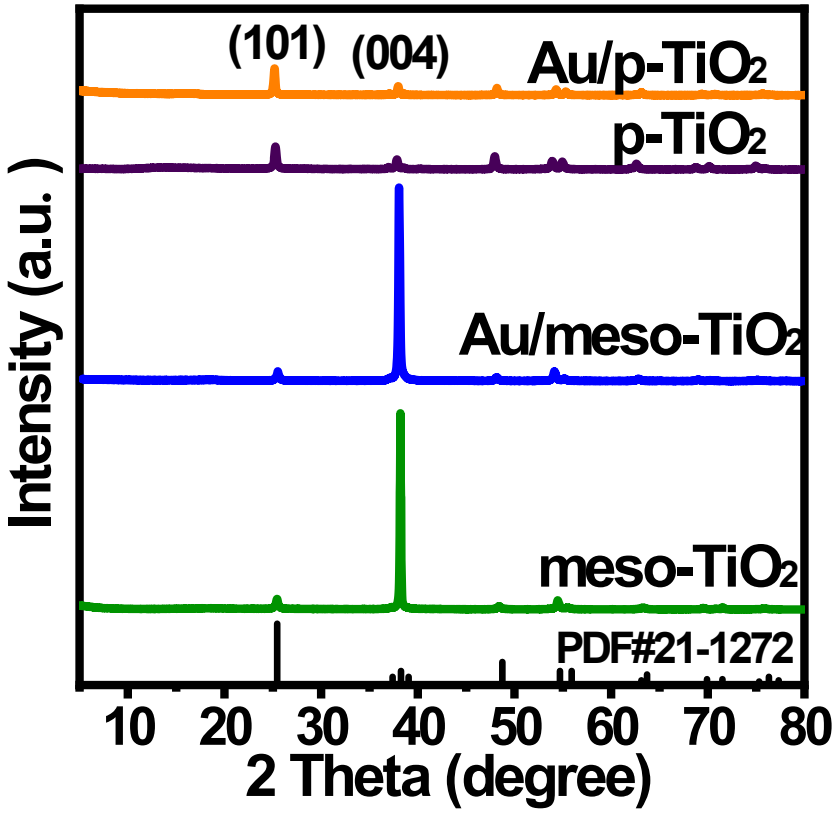

Fig. S2. XRD patterns of meso-TiO_2, p-TiO_2, Au/meso-TiO_2 and Au/p-TiO_2.

As shown in **Fig. S2**, the XRD peaks of meso-TiO_2, p-TiO_2, Au/meso-TiO_2, and Au/p-TiO_2 can be indexed to the tetragonal anatase phase of TiO_2 (JCPDS no. 21-1272). Loading Au nanoparticles to meso-TiO_2 and p-TiO_2 did not cause any obvious changes to the crystallinity of TiO_2.

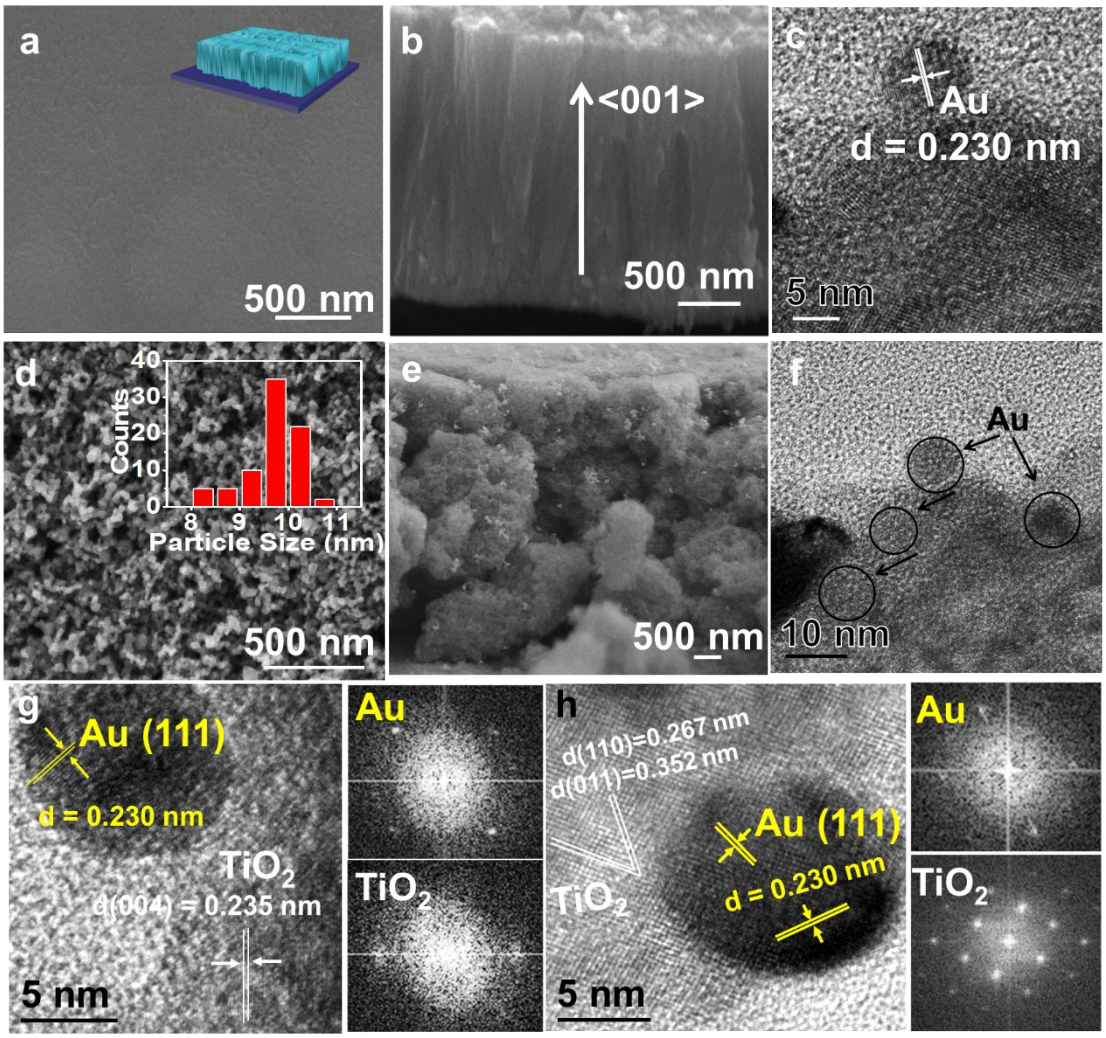

Fig. S3. (a) Top-view SEM image and (b) side-view image of meso-TiO_2, and (c) HRTEM image of Au/p-TiO_2. (d) Top-view SEM image and size distributions of Au, and (e) side-view image of Au/P25. (f) HRTEM image of Au/P25. (g, h) High-resolution TEM image of Au/meso-TiO_2.

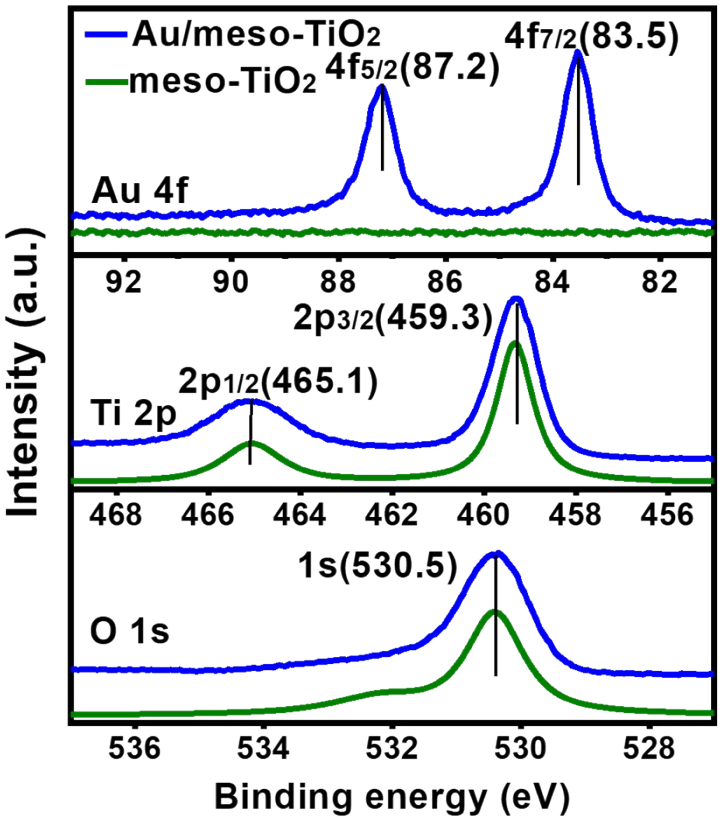

Fig. S4. XPS spectra of Au/meso-TiO_2 and meso-TiO_2 samples.

The XPS spectra of Au/meso-TiO_2 in **Fig. S4** show the signal of Au 4*f* and those of Ti 2*p* and O 1*s* elements. The high-resolution spectrum of Au 4*f* exhibits two peaks at 83.5 eV (Au $4f_{7/2}$) and 87.2 eV (Au $4f_{5/2}$), which can be assigned to metallic Au. The binding energies of 459.3 and 465.1 eV can be ascribed to Ti $2p_{3/2}$ and Ti $2p_{1/2}$, respectively. The peaks for Ti 2*p* and O 1*s* of Au/meso-TiO_2 are consistent with meso-TiO_2. The results confirmed the metallic state of the Au NPs in the Au/meso-TiO_2.

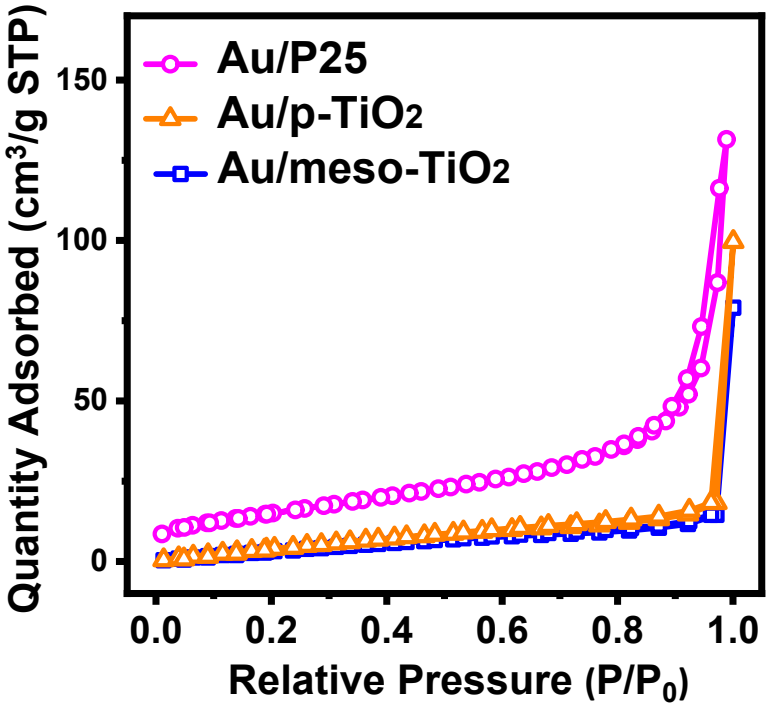

Fig. S5. Nitrogen adsorption/desorption isotherms of Au/meso-TiO_2, Au/p-TiO_2 and Au/P25.

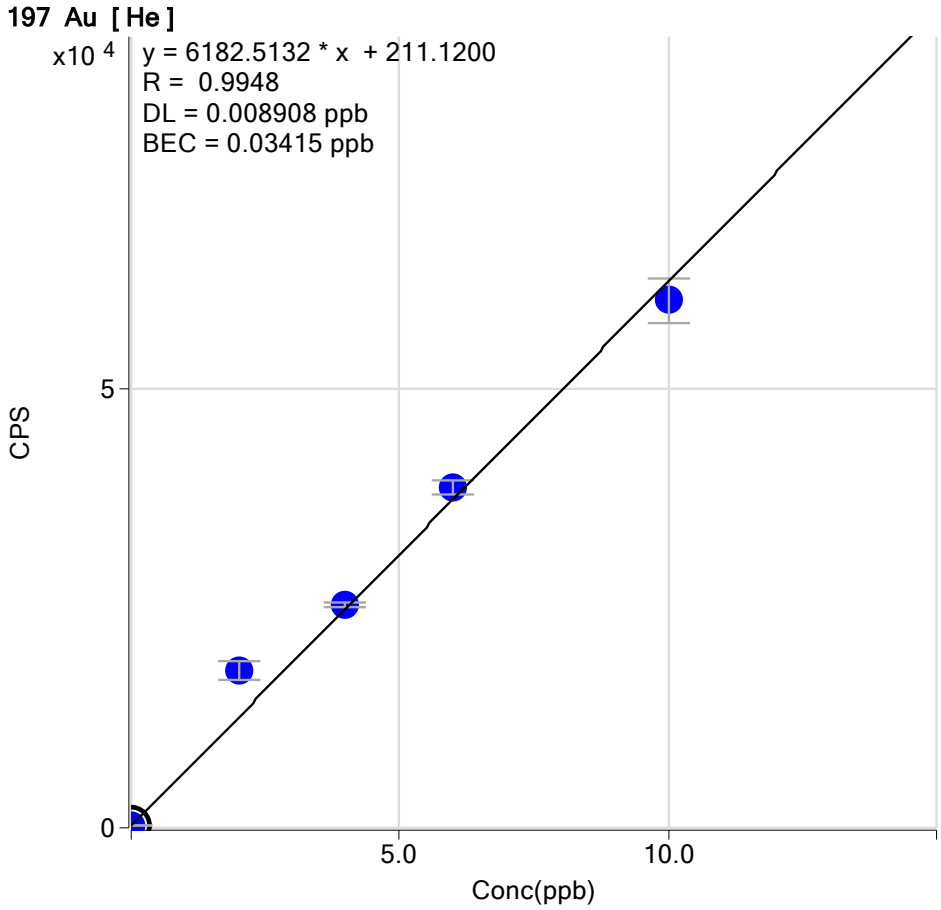

Fig. S6. The standard curve of Au concentration measured by ICP-MS.

The solutions for the ICP-MS experiment were prepared in the following manner: 5 mg of sample dissolved in 5 mL of aqua regia solution, optimally in a molar ratio of 1:3, then 10 μL of the solution was taken out and diluted into 250 mL of 2.0 % (v/v) HNO_3 aqueous solution. As shown in Fig. S6 and Table S1, the Au content is 2.0 wt.% in Au/meso-TiO_2, 2.0 wt.% in Au/p-TiO_2, and 2.1 wt.% in Au/P25, respectively. The results indicate that the amount of Au loading in the as-synthesized samples is almost identical.

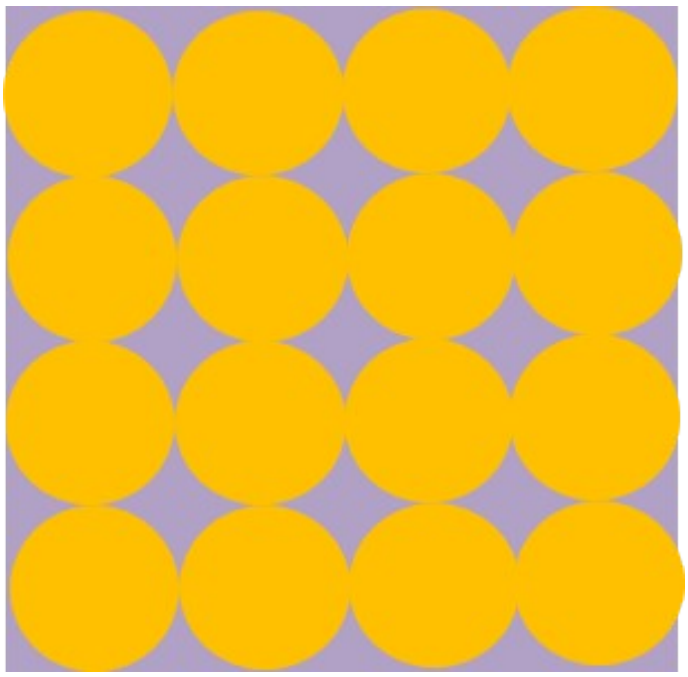

Fig. S7. The model of Au NPs arrangement uses for light transmission calculation.

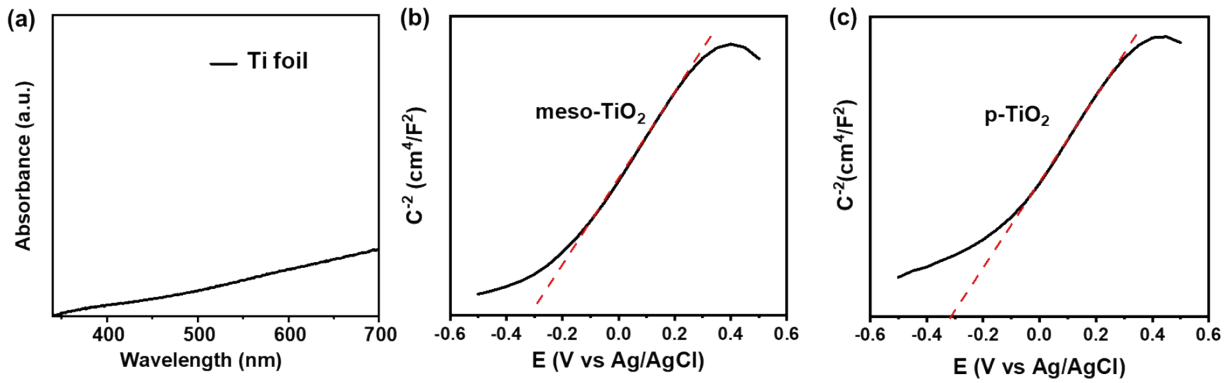

Fig. S8. (a) UV-vis absorption spectra of Ti foil. Mott−Schottky plots for (b) meso-TiO_2 and (c) p-TiO_2 at a frequency of 1 k Hz obtained in darkness.

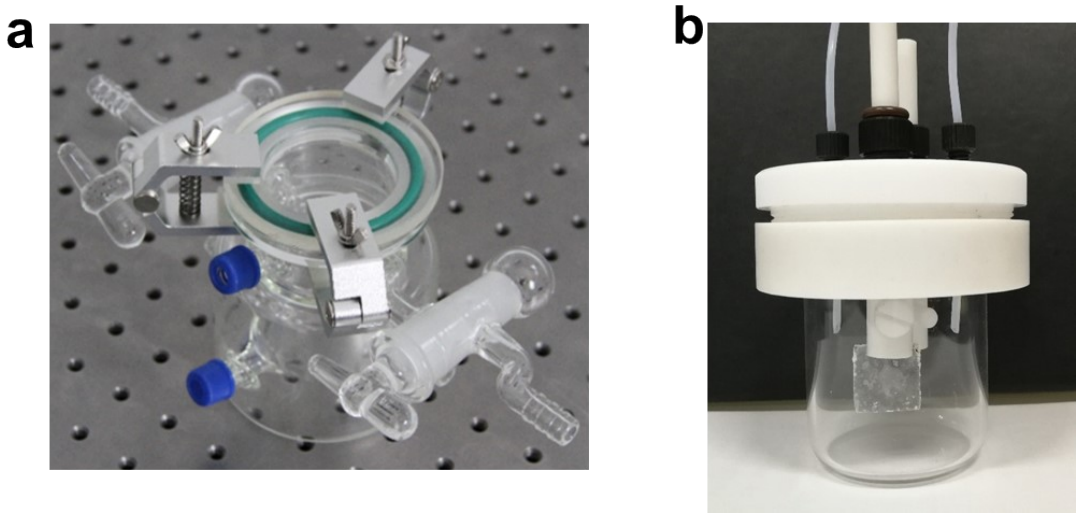

Fig. S9. Photographs of the photocatalysis equipment used for (a) water splitting and for (b) gaseous CH_3SH oxidation, respectively.

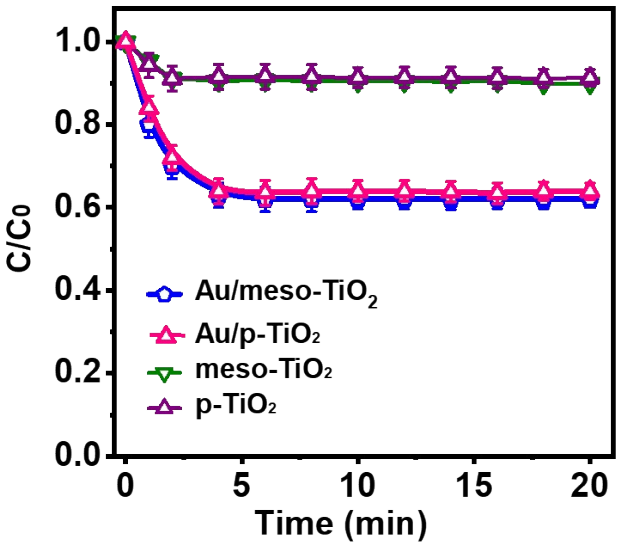

Fig. S10. The CH_3SH adsorption performance of the as-synthesized samples under darkness.

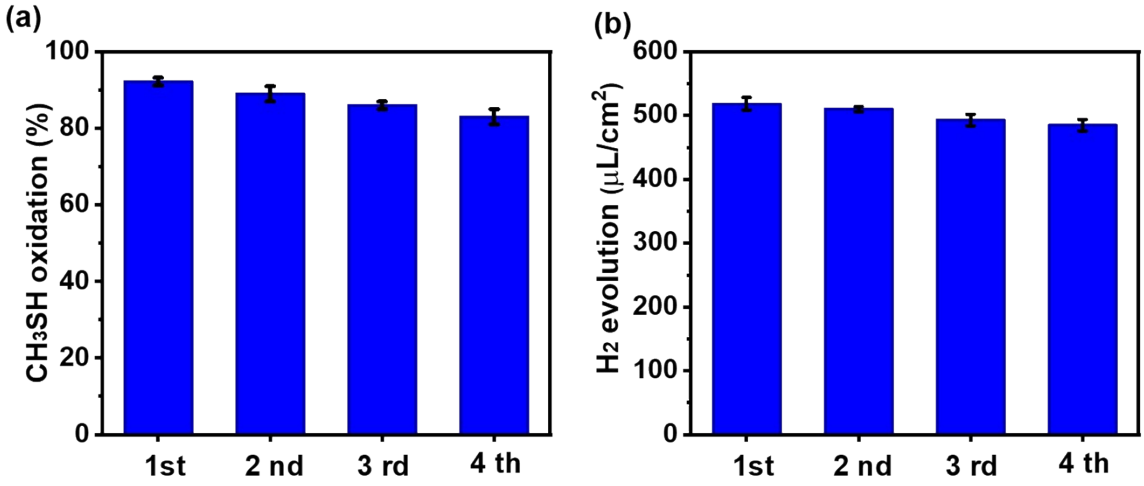

Fig. S11. Cycling performance of Au/meso-TiO_2 for the (a) removal of odorous CH_3SH and (b) H_2 evolution.

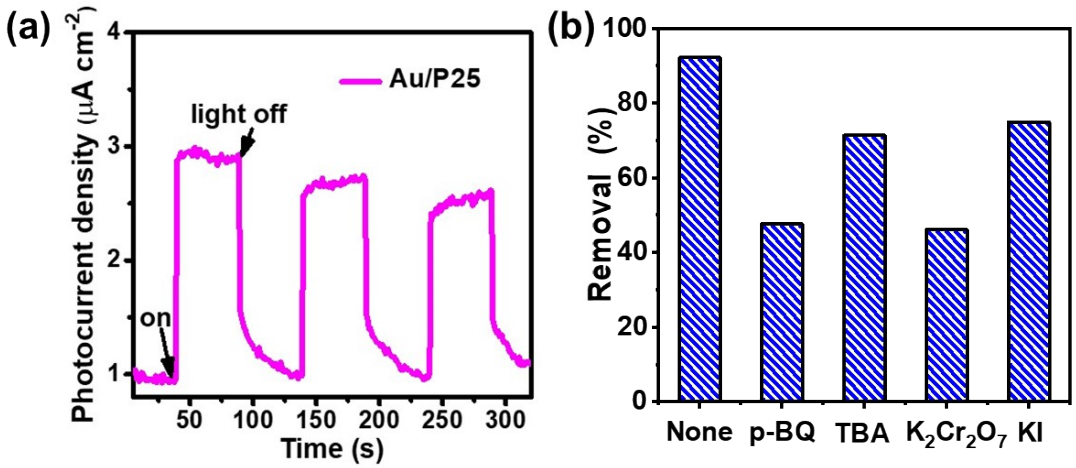

Fig. S12. (a) Photocurrent responses of Au/P25 at an applied potential of 0.8 V *vs.* Ag/AgCl in 0.5 M Na_2SO_4 aqueous solutions under visible-light irradiation (λ > 430 nm). (b) Reaction suppression by the chemical scavengers of reactive species $\bullet O_2^-$, •OH, e^- and h^+.

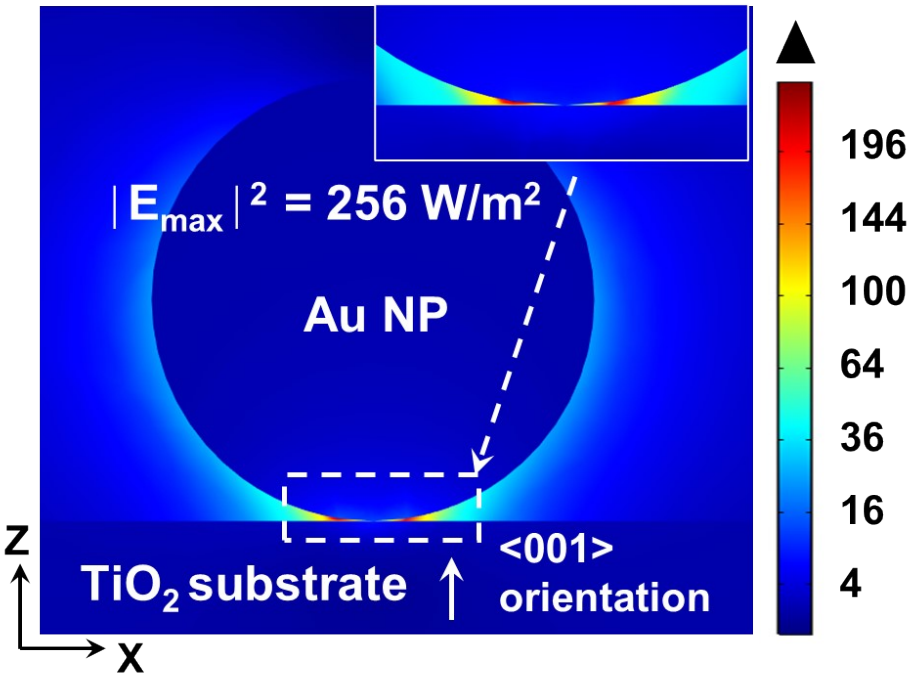

Fig. S13. Normalized electric field intensity distributions in the xz plane at 540 nm for Au NPs on <001> oriented anatase TiO_2.

Supplemental References

1. Yang, J., Wu, Q., He, S., Yan, J., Shi, J., Chen, J., Wu, M., and Yang, X. *Nanoscale* **2015,** *7*, 13888-13897.
2. Segall, M., Lindan, P.J., Probert, M.a., Pickard, C.J., Hasnip, P.J., Clark, S., and Payne, M. *J. Phys. Condens. Matter* **2002,** *14*, 2717.
3. Knight, M.W., Wu, Y., Lassiter, J.B., Nordlander, P., and Halas, N.J. *Nano Lett.* **2009,** *9*, 2188-2192.
4. Wang, J., Ando, R.A., and Camargo, P.H.C. *Angew. Chem. Int. Ed.* **2015**, *54*, 6909-6912.
5. Jellison Jr, G., Boatner, L., Budai, J., Jeong, B.-S., and Norton, D. *J. Appl. Phys.* **2003**, *93*, 9537-9541.
6. Chen, C.-Y., Wang, J.-Y., Tsai, F.-J., Lu, Y.-C., Kiang, Y.-W., and Yang, C. *Opt. Express* **2009,** *17*, 14186-14198.
7. Zhang, J., Jin, X., Morales-Guzman, P.I., Yu, X., Liu, H., Zhang, H., Razzari, L., and Claverie, J.P. *ACS Nano* **2016,** *10*, 4496-4503.
8. Xia, D., Xu, W., Wang, Y., Yang, J., Huang, Y., Hu, L., He, C., Shu, D., Leung, D.Y.C., and Pang, Z. *Environ. Sci. Technol.* **2018,** *52*, 13399-13409.
9. Hu, L., He, H., Xia, D., Huang, Y., Xu, J., Li, H., He, C., Yang, W., Shu, D., and Wong, P.K. *ACS Appl. Mater. Interfaces* **2018,** *10*, 18693-18708.
10. Yang, J., Zhang, Q., Zhang, F., Xia, D., Liu, H., Tian, S., Sun, L., Shu, D., He, C., and Runa, S. *J. Hazard. Mater.* **2018,** *358*, 136-144.
11. Sano, T., Koike, K., Hori, T., Hirakawa, T., Ohko, Y., and Takeuchi, K. *Appl. Catal. B* **2016,** *198*, 133-141.
12. Zhao, Y., Chen, D., Liu, J., He, D., Cao, X., Han, C., Lu, J., and Luo, Y. *Chem. Eng. J.* **2020,** *389*, 124384.
13. Chou, A., Jaatinen, E., Buividas, R., Seniutinas, G., Juodkazis, S., Izake, E.L., and Fredericks, P.M. *Nanoscale* **2012,** *4*, 7419-7424.
14. Fusco, Z., Rahmani, M., Bo, R., Verre, R., Motta, N., Käll, M., Neshev, D., and Tricoli, A. *Adv. Mater.* **2018,** *30*, 1800931.